

Observation of finite excess noise in the voltage-biased quantum Hall regime as a precursor for breakdown

Kensaku Chida,^{1,*} Tomonori Arakawa,¹ Sadashige Matsuo,¹ Yoshitaka Nishihara,¹ Takahiro Tanaka,¹ Daichi Chiba,¹ Teruo Ono,¹ Tokuro Hata,² Kensuke Kobayashi,^{1,2} and Tomoki Machida^{3,4},

¹*Institute for Chemical Research, Kyoto University, Uji, Kyoto 611-0011, Japan*

²*Graduate School of Science, Osaka University, 1-1 Machikaneyama, Toyonaka, Osaka 560-0043, Japan.*

³*Institute of Industrial Science, University of Tokyo,
4-6-1 Komaba, Meguro-ku, Tokyo 153-8505, Japan and*

⁴*Institute for Nano Quantum Information Electronics,
University of Tokyo, 4-6-1 Komaba, Meguro-ku, Tokyo 153-8505, Japan*

(Dated: June 5, 2019)

We performed noise measurements in a two-dimensional electron gas to investigate the nonequilibrium quantum Hall effect (QHE) state. While excess noise is perfectly suppressed around the zero-biased QHE state reflecting the dissipationless electron transport of the QHE state, considerable finite excess noise is observed in the breakdown regime of the QHE. The noise temperature deduced from the excess noise is found to be of the same order as the energy gap between the highest occupied Landau level and the lowest empty one, supporting the idea that avalanche-type electron heating occurs. Moreover, unexpected finite excess noise is observed at a finite source-drain bias voltage smaller than the onset voltage of the QHE breakdown, which may be called the “precursor regime.” The excess noise in this precursor regime is reproducibly observed at different filling factors and cooling downs. In addition, it shows unique temporal variation on a time scale of ten minutes. Such a slow dynamics of the excess noise in the precursor regime is proposed to originate from the electron tunneling between the edge states and the localized bulk states.

PACS numbers: 73.43.-f, 73.43.Fj, 73.50.Td, 72.20.Ht

I. INTRODUCTION

A two-dimensional electron gas (2DEG) under the influence of a large perpendicular magnetic field exhibits a remarkable dissipationless state with precisely quantized Hall resistance, which is the integer quantum Hall effect (QHE),¹ as a consequence of the topological rigidity of the phase.² The existence of the localized bulk states plays an essential role in the precise quantization of the Hall resistance.³ They spatially separate the counterflowing channels at the sample edge to strongly suppress backscattering.⁴ More precisely, the edge channels are regarded as “incompressible strips” owing to the electron screening.^{5,6} Although the nature of the QHE state is successfully explained by the topological rigidity, details of the state in nonequilibrium are largely unexplored. Recent experiments aimed at quantum information processing by using edge channels, involving phase reversal of electrons in electron interferometers,^{7,8} decoherence,^{9–14} energy relaxation,^{15–17} and dynamics of the edge magnetoplasmons in the edge channels,^{18,19} have clarified electron behaviors in the nonequilibrium QHE state. Thus, detailing the nonequilibrium properties of the QHE states has become an important research topic in present condensed-matter physics.

The longstanding problem of the nonequilibrium QHE state called as the QHE breakdown has vexed metrology researchers for about three decades. The quantized Hall resistance collapses at finite source drain voltage (V_{sd}) and/or at a current larger than a certain value.^{20,21} The QHE breakdown is, in other words, a transition from

a topologically protected phase to a completely different one. For this reason, the importance of the QHE breakdown has invoked renewed interest as new types of topologically protected phases,²² that is, topological insulators, have gathered much attention today. As the topological insulator phase is a scion of the QHE state, a detailed understanding on how the QHE state breaks down should shed new light on the robustness of the topologically protected phases.

A number of mechanisms for the QHE breakdown have been proposed thus far^{23–31}, and results of experiments have revealed substantial properties of the breakdown, including electron overheating through the avalanche-type electron scattering,^{32,33} the spatial gradient of the effective electron temperature along the electron path³⁴, the typical length of the electron heating and cooling,^{35,36} and the time scale of the breakdown.^{37,38} Although these experiments have uncovered important information regarding the QHE breakdown, its mechanism remains to be clarified.³⁹

Noise measurement is a promising candidate that can provide highly significant information on the QHE breakdown. In fact, it has revealed various unique properties of electron transport⁴⁰ that could not be obtained through conventional conductance and resistance measurements. In the QHE state, the excess noise is suppressed because of the absence of backscattering.⁴¹ Hence, we expect that we can detect the QHE breakdown by investigating the mechanism through which excess noise occurs. The excess noise may provide us with direct information on the effective electron temperature, which can

be compared to the values calculated from the longitudinal resistance.^{32,33} To the best of our knowledge, there has been no experimental work that has studied these aspects.

In this work, we present the experimental results of the noise measurement to clarify the QHE breakdown mechanism. Two distinct observations are made. The first one is that the electron heating accompanied by the breakdown is of the order of the energy gap between the highest occupied Landau level and the lowest unoccupied one. This fact supports the idea that avalanche-type electron heating occurs, being induced by the electron scattering between the Landau levels. Second, unexpectedly, we observed finite excess noise prior to the QHE breakdown at a finite V_{sd} that is smaller than the onset voltage of the QHE breakdown (a V_{sd} region that we define as a precursor regime), indicating the presence of finite dissipation in the nonequilibrium QHE states. The excess noise shows a unique temporal variation on a scale of minutes.

We propose that such a slow dynamics of the excess noise reflects the electron tunneling between the edge state and the bulk localized states. The long time scale of the temporal variation indicates a weak but finite coupling between the edge states and the localized bulk states. Because such an effect has not been observed in conventional conductance or resistance measurements, the noise measurement would be a useful probe to investigate the coupling between the edge state and the localized bulk states.

This paper is organized as follows. In Sec. II, we describe our device and the experimental setup used for high-frequency (2.55 MHz) and low-frequency (1–100 kHz) noise measurements. In Sec. III A, we present the experimental results of the noise measurements, and using the results, we deduce the effective electron temperature in the breakdown regime of the QHE. In Sec. III B, we discuss the temporal variation of the excess noise in the precursor regime. Then, in Sec. III C, we propose a possible mechanism for the slow dynamics of the excess noise in the precursor regime. In Sec. IV, we summarize our work.

II. EXPERIMENT

A. Device

The QHE breakdown was investigated using a two-terminal device fabricated on a semiconductor with a 2DEG in an AlGaAs/GaAs interface. The 2DEG has electron density $n_e = 2.3 \times 10^{15} \text{ m}^{-2}$ and mobility $\mu = 110 \text{ m}^2/(\text{Vs})$. The geometry of the two-terminal device is schematically shown in Fig. 1(a). The Hall bar with width $W = 40 \text{ }\mu\text{m}$ is fabricated by wet etching. Then, the main part of the device is defined by the negatively charged gate electrodes to have $W = 20 \text{ }\mu\text{m}$ and length $L = 300 \text{ }\mu\text{m}$. As Kaya *et al.* reported

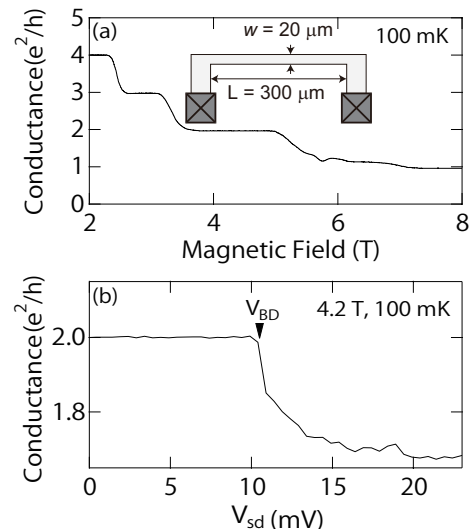


FIG. 1. (a) Equilibrium conductance of the device as a function of B and schematic illustration of the present two-terminal device. (b) Differential conductance of the device as a function of V_{sd} . V_{BD} is defined as V_{sd} at which $\Delta G = G(V_{sd}) - G(0) = 0.01e^2/h$.

previously,^{35,36} the narrow constriction of the main part is utilized for inducing the QHE breakdown specifically at the entrance of the main part.

The basic properties of the device were checked by a conductance measurement at equilibrium with the standard lock-in technique with excitation voltage of $10 \text{ }\mu\text{V}$ at 37 Hz . Figure 1(a) shows the differential conductance of the device $[G(V_{sd})]$ as a function of a magnetic field perpendicular to the 2DEG (B) at electron temperature $T = 100 \text{ mK}$. The clear conductance plateaus at e^2/h , $2e^2/h$, $3e^2/h$, and $4e^2/h$ represent the QHE with Landau level filling factors of $\nu = 1, 2, 3$, and 4 , respectively. At the conductance plateaus, the conductance remains quantized up to the finite source-drain bias voltage V_{sd} smaller than a certain critical value. Figure 1(b) shows $G(V_{sd})$ as a function of V_{sd} at $B = 4.2 \text{ T}$ ($\nu = 2.1$); the curve exhibits an abrupt conductance collapse from $2e^2/h$ at $V_{sd} = 10.4 \text{ mV}$. In this paper, the onset voltage of the QHE breakdown (V_{BD}) is defined as the V_{sd} value at which the conductance deviation $\Delta G(V_{sd}) = G(0) - G(V_{sd})$ exceeds $0.01e^2/h$. We call the V_{sd} region $|V_{sd}| < |V_{BD}|$ the “QHE regime” and call the $|V_{sd}| > |V_{BD}|$ region the “breakdown regime.” We focus on the results obtained with the etching defined edge as it exhibits a more distinctive QHE breakdown than the electrically defined one.⁴²

B. Noise measurement and its analysis

To obtain the noise spectral density of the device, a high-frequency ($\sim\text{MHz}$) noise measurement setup and a low-frequency ($\sim\text{kHz}$) noise measurement setup were uti-

lized. The former adopts a resonator to obtain information at a frequency that is sufficiently high to prevent $1/f$ noise, by focusing on a specific frequency defined by the resonator. The latter enables us to obtain the frequency dependence of the noise spectral density, although the bandwidth is limited to less than 100 kHz owing to RC damping. From the noise spectrum for a wide frequency range below 100 kHz, the contribution of low-frequency noise such as $1/f$ noise is evaluated. In the subsequent text, we describe the measurement scheme and analysis in further detail.

1. High-frequency measurements

A schematic illustration of the high-frequency noise measurement setup and the noise spectra obtained with the setup are shown in Fig. 2(a) and (b), respectively. The measurement is performed in a dilution refrigerator by utilizing an LC resonator with a peak frequency f_0 of 2.55 MHz and a homemade cryogenic amplifier as we reported previously.^{43–45} As shown in Fig. 2(b), the resonant peak at 2.55 MHz is larger for the biased case ($V_{sd} = 15$ mV) than in the equilibrium case ($V_{sd} = 0$ mV). The difference is mainly due to the excess noise. We evaluate the resonant peak by using the following Lorentzian-like function:^{46,47}

$$P(f) = P_B + \frac{P_0}{1 + (f^2 - f_0^2)^2 / (f\Delta f)^2}, \quad (1)$$

where P_B is the frequency-independent background noise, P_0 is the peak height of the Lorentzian-like function, f_0 is the peak frequency, and Δf is the full width at half maximum. By evaluating Δf using the equation $\Delta f = (1/2\pi C)[G(V_{sd}) + 1/Z]$, the capacitance C and the impedance Z of the setup are estimated to be 120 pF and 70 k Ω , respectively.^{47,48} The noise spectral density of the device is obtained from the following conventional

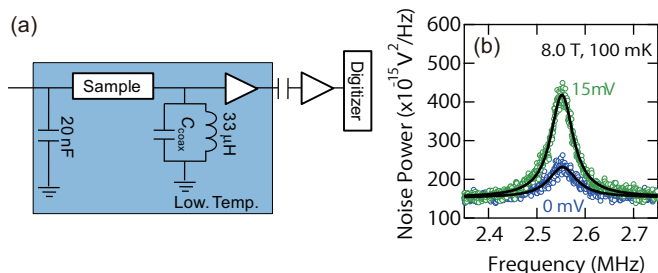


FIG. 2. (Color online) (a) Schematic illustration of the two-terminal device and setup for the high-frequency noise measurements. (b) Noise spectra with a resonant peak at 2.55 MHz obtained at $V_{sd} = 0$ and 15 mV. The solid curves are the result of the fitting by Eq. (1).

equation:⁴⁰

$$P_0(V_{sd}) = A \left(S_V^{\text{out}} + \left(\frac{ZR}{Z+R} \right)^2 S_I^{\text{out}} + \left(\frac{ZR}{Z+R} \right)^2 S_{\text{dev}}(V_{sd}) \right), \quad (2)$$

where A is the square of the total gain of the amplifier system and S_V^{out} and S_I^{out} are the voltage and current noise generated by the cryogenic amplifier, respectively. $R = 1/G$ is the resistance of the device and $S_{\text{dev}}(V_{sd})$ is the current noise generated at the device, which consists of thermal noise $S_{\text{th}} = S_{\text{dev}}(0)$ and excess noise $S(V_{sd}) = S_{\text{dev}}(V_{sd}) - S_{\text{dev}}(0)$. The setup is calibrated by measuring $S_{\text{th}} = 4k_B T G(0)$ at equilibrium with a quantum point contact on the same device, where k_B is the Boltzmann constant. The obtained parameters of the setup are $A = 3.5 \times 10^5$, $S_V^{\text{out}} = 1.0 \times 10^{-19}$ V²/Hz, and $S_I^{\text{out}} = 1 \times 10^{-28}$ A²/Hz, and the base electron temperature of the dilution refrigerator is $T \sim 100$ mK.⁴⁹

Because the resonant frequency of the resonator is on the scale of megahertz, which is usually sufficiently high to damp the $1/f$ noise, the resonant peak is expected to be attributed to only the white noise. However, to ensure that the obtained spectral density is free from any frequency-dependent noise contribution, we need to examine spectral density behavior over a wide frequency range, as discussed in the following text.

2. Low-frequency measurements

To evaluate a possible contribution of the $1/f$ noise to the excess noise at 2.55 MHz, the noise spectrum in the range from 1 to 100 kHz is obtained with a variable temperature insert (VTI) as in previous experiments.^{46,50–52} The cross-correlation technique is employed as shown in Fig. 3(a) to minimize the external noise from the cables and the amplifiers. Figure 3(b) shows $P(f)$ obtained in the QHE regime ($V_{sd} = 0$ mV) and the breakdown regime

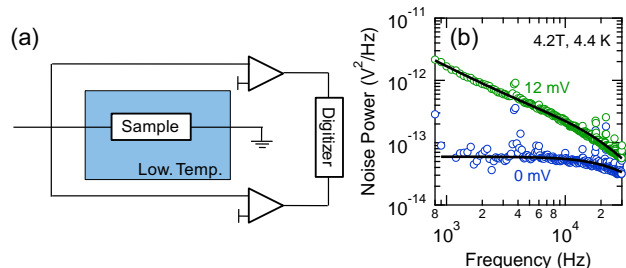


FIG. 3. (Color online) (a) Schematic illustration of the setup for the low-frequency noise measurement utilizing the cross-correlation technique. (b) Noise spectra in the kilohertz range obtained at $V_{sd} = 0$ and 12 mV. The solid curves are the result of the fitting by Eq. (3).

($V_{sd} = 12$ mV). RC damping is obvious for frequencies above 20 kHz. We have confirmed that the obtained noise above 1 kHz is composed of the intrinsic noise of the present device caused by the long time averaging in the cross-correlation method. In the QHE regime, the excess noise in the frequency range from 1 to 20 kHz is frequency independent. However, $1/f$ contribution of the noise is observed in the breakdown regime. Thus, the noise spectrum is expressed by the following equation:

$$P(f) = A \left(S_V^{\text{dev}}(V_{sd}) + \frac{a(V_{sd})}{f} \right) \left(\frac{1}{1 + (2\pi fCR)^2} \right), \quad (3)$$

where $S_V^{\text{dev}}(V_{sd}) = R^2 S_{\text{dev}}(V_{sd})$ is the contribution of the frequency-independent noise, $a(V_{sd})/f = R^2 S_{1/f}(V_{sd})$ is that of the $1/f$ noise, and $1/[1 + (2\pi fCR)^2]$ represents the RC damping with a cutoff frequency of $f_c = 1/2\pi CR$. The curve fitting is performed in the frequency range between 1 and 50 kHz. The equilibrium noise measurement determines A , C , and the base electron temperature for the measurement setup as 1.044×10^4 , 400 pF, and 4.4 K, respectively.

III. RESULTS AND DISCUSSION

A. Estimation of the noise temperature

The excess noise at 2.55 MHz is converted to noise temperature $T_N = S(V_{sd})/4k_B G(V_{sd})$ to study the electron heating accompanied by the QHE breakdown. In addition, we evaluate the contribution of the $1/f$ noise at 2.55 MHz from the noise spectra obtained from the low-frequency noise measurement to exclude the contribution of unintended low-frequency noise on $S(V_{sd})$ at 2.55 MHz. In the next subsection, the noise temperature in the breakdown regime is discussed with a combination of high-frequency and low-frequency noise measurements.

1. High-frequency measurements

Figure 4(a) shows $G(V_{sd})$ as a function of V_{sd} at $B = 4.2$ ($\nu = 2.1$), 5.6 ($\nu = 1.6$), and 8.0 T ($\nu = 1.1$). In the $\nu = 2$ QHE state ($B = 4.2$ T), $G(V_{sd})$ shows quantization as $2e^2/h$ at V_{sd} up to $V_{sd} = 10.4$ mV. At $V_{sd} = 10.4$ mV = V_{BD} , $G(V_{sd})$ abruptly deviates from the quantized value because of the QHE breakdown. At V_{sd} larger than V_{BD} , $G(V_{sd})$ is smaller than $2e^2/h$ owing to presence of electron scattering. The same features are also observed in the $\nu = 1$ QHE state ($B = 8.0$ T). In this case, $G(V_{sd})$ is quantized as e^2/h and $V_{BD} = 2.0$ mV. In contrast, in the transition between the two QHE states ($B = 5.6$ T), $G(V_{sd})$ does not exhibit any conductance quantization around $V_{sd} = 0$ mV.

Figure 4(b) shows $S(V_{sd})$ as a function of V_{sd} , which is simultaneously obtained with $G(V_{sd})$ in Fig. 4(a). In the QHE states ($B = 8.0$ and 4.2 T), $S(V_{sd})$ is strongly

suppressed at $V_{sd} < V_{BD}$, reflecting the edge transport of the QHE state with the strong suppression of backscattering. At $V_{sd} = V_{BD}$, an abrupt increase in the excess noise is observed; this is explicit evidence of the transition between the dissipationless state and the dissipative one.

In the transition of the QHE states ($B = 5.6$ T), $S(V_{sd})$ is very small. The nominal Fano factor $F = S(V_{sd})/2eV_{sd}G(V_{sd})$ is 5×10^{-4} , which indicates that our device is sufficiently macroscopic to exclude any shot noise contribution to the excess noise. Note that the device length is much larger than the mean free path of the 2DEG, $l \sim 12$ μm .

Now, we assume that the electron heating in the breakdown regime can be regarded as $T_N(V_{sd})$ (the validity of which is discussed in later text). In the even-integer QHE state, T_N is deduced as ~ 10 K using the typical values of $G(V_{sd})$ and $S(V_{sd})$ in the breakdown regime: $\sim 1.8e^2/h$ and 30×10^{-27} A²/Hz [see Fig. 4(a) and 4(b)]. In the odd-integer QHE state, T_N is about 1 K for the typical values of $G(V_{sd})$ and $S(V_{sd})$ in the breakdown regime: $\sim 0.8e^2/h$ and 1.0×10^{-27} A²/Hz [see Fig. 4(a) and 4(b)].

We found that the obtained $T_N(V_{sd})$ in the breakdown regime is of the order of the energy gap between the Landau levels. In the odd-integer QHE case, the energy gap is determined by the Zeeman energy $E_Z = g\mu_B B$, where g is the electron g factor of bulk GaAs and μ_B is the Bohr magneton. E_Z is about 2 K at $B = 8.0$ T and the obtained T_N at $B = 8.0$ T is about 1 K. In the even-integer QHE case, the energy gap is determined by the cyclotron angular frequency $E_c = \hbar\omega_c$, where \hbar is the Dirac constant and ω_c is the cyclotron energy. At 4.2 T, $E_c \sim 35$ K and T_N is deduced as ~ 10 K. This $T_N(V_{sd})$ behavior supports the idea that the QHE breakdown occurs, induced by avalanche-type electron scattering, that

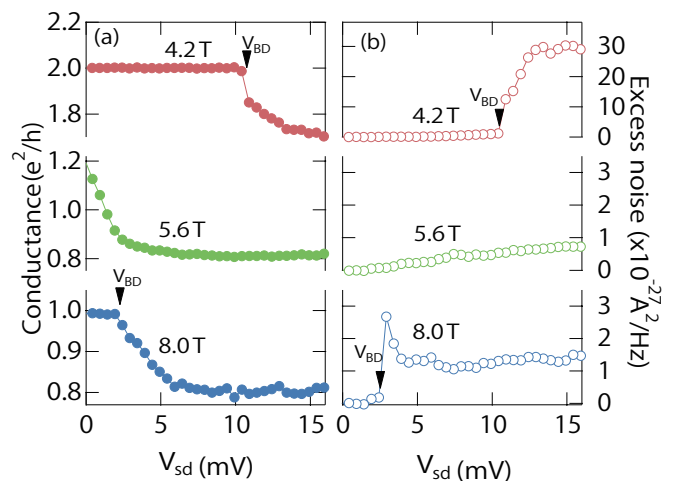


FIG. 4. (Color online) (a) G as a function of V_{sd} . (b) S as a function of V_{sd} . Measurements are performed at $B = 4.2, 5.6,$ and 8.0 T ($\nu = 2.1, 1.6,$ and 1.1 , respectively) and $T = 100$ mK.

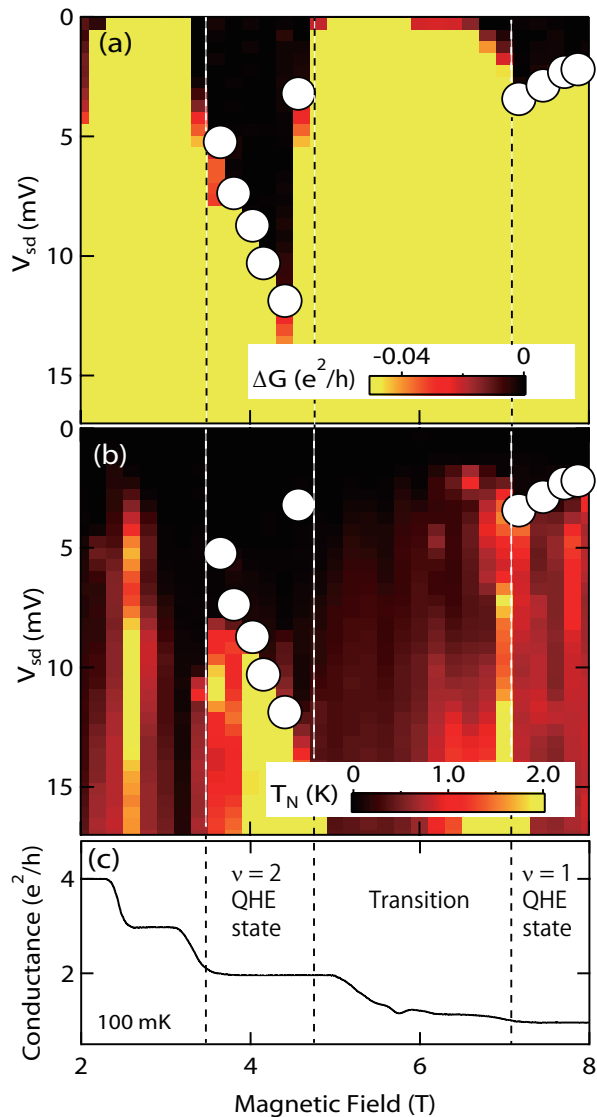


FIG. 5. (Color online) (a) Color plot of $\Delta G = G(V_{sd}) - G(0)$ as a function of B and V_{sd} . (b) Color plot of T_N as a function of B and V_{sd} . (c) Equilibrium conductance as a function of B . The open circles in (a) and (b) indicate V_{BD} at each field.

develops into electron heating of the order of the energy gap between the Landau levels.³³

Figure 5(a) shows a color plot of the conductance deviation from the equilibrium value $\Delta G(V_{sd}) = G(V_{sd}) - G(0)$ as a function of B and V_{sd} . $\Delta G(V_{sd}) = 0$ at a small finite V_{sd} around 4 and 8 T, which reflects the conductance quantization of the QHE state. In the transition between the QHE states [5–7 T; see Fig. 5(c)], $G(V_{sd})$ does not have a conductance plateau [$\Delta G(V_{sd}) \neq 0$ at a small V_{sd}]. The QHE breakdown is observed as an abrupt collapse of the quantized conductance at finite V_{sd} . The open circles in Fig. 5(a) and (b) indicate V_{BD} at each field.

Figure 5(b) shows a color plot of $T_N(V_{sd})$ as a function of B and V_{sd} . In the $\nu = 1$ QHE state (around 8 T), be-

cause the QHE state is dissipationless, $T_N(V_{sd})$ is almost zero around $V_{sd} = 0$ mV. After the QHE breakdown, at V_{sd} larger than V_{BD} , $T_N(V_{sd})$ is about 1 K owing to electron heating through avalanche-type electron scattering. In the transition of the QHE states (around 6 T), the excess noise is rather low, owing to the absence of avalanche-type electron scattering. In the $\nu = 2$ QHE state (around 4 T), the excess noise is strongly (but not perfectly) suppressed when the conductance is quantized. After the QHE breakdown, $T_N(V_{sd})$ increases abruptly to about 10 K.

2. Low-frequency measurements

The above estimation of $T_N(V_{sd})$ was based on the assumption that the excess noise is frequency independent. We validate this assumption with the noise spectrum obtained by using the low-frequency noise measurement setup. Unfortunately, the noise spectrum is only obtained at 4.4 K because of our experimental setup. However, empirically, the $1/f$ noise increases when the temperature increases. Therefore, the $1/f$ noise amplitude at 4.4 K gives us the upper bound of the $1/f$ noise contribution at 100 mK.

Figure 6(a) shows the equilibrium conductance of the device as a function of B obtained with the low-frequency noise measurement setup. Because the thermal fluctuation at 4.4 K is larger than the Zeeman energy ($E_z \sim 2$ K at 8.0 T), the plateau of the $\nu = 1$ QHE state is absent (not shown). The noise spectrum was well reproduced with Eq. (3) [see Fig. 3(b)]. Thus, the excess noise is composed of two components: the frequency-independent noise and the $1/f$ noise.

Before evaluating the $1/f$ noise contribution on the excess noise at 2.55 MHz, it is worth considering the frequency-independent component of the excess noise $S(V_{sd}) = S_{dev}(V_{sd}) - S_{dev}(0)$. In the $\nu = 2$ QHE state (around 4.0 T), $S(V_{sd})$ is strongly suppressed at a V_{sd} smaller than 8 mV, reflecting the presence of dissipationless edge transport of the QHE state. At $V_{sd} = 10.0$ mV, $S(V_{sd})$ is about 20×10^{-27} A²/Hz and it is estimated as $T_N(V_{sd}) \sim 7$ K. The estimated value of $T_N(V_{sd})$ is consistent with the value obtained from the high-frequency noise measurement.

Figure 6(b) shows a color plot of the $1/f$ noise amplitude $a(V_{sd})$ as a function of V_{sd} and B . The maximum value of $a(V_{sd})$ is observed at $B = 3.6$ T and $V_{sd} = 15$ mV and is about 6×10^{-13} V². From the maximum value of $a(V_{sd})$, the $1/f$ noise amplitude at 2.55 MHz is estimated as 1.2×10^{-27} A²/Hz by using the empirical relation $S_{1/f}(f) = G(V_{sd})^2 a/f$, which is less than a few percent of the excess noise in the breakdown regime at the $\nu = 2$ QHE state ($\sim 30 \times 10^{-27}$ A²/Hz). Because the $1/f$ noise is empirically reduced by the temperature decrease, the estimation of the noise temperature from the excess noise is justified.

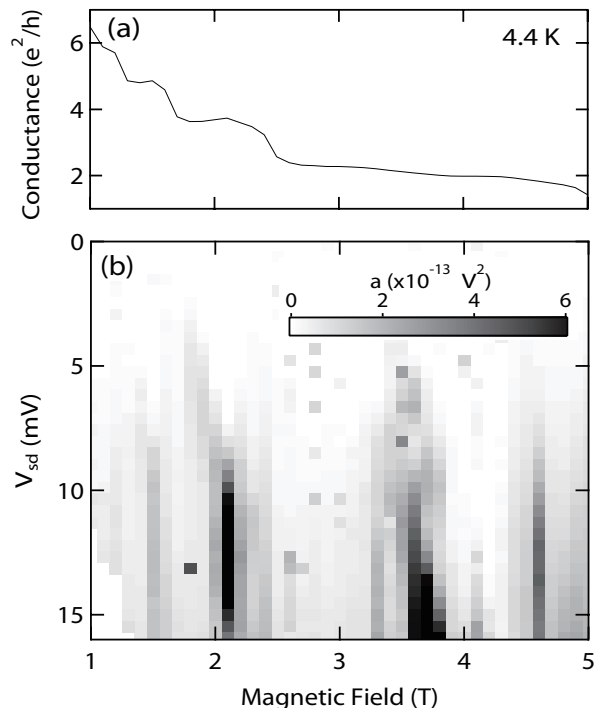


FIG. 6. (Color online) (a) Equilibrium conductance as a function of B at $T = 4.4$ K. (b) Color plot of $a(V_{sd})$ as a function of V_{sd} and B .

B. Observation of the precursor phenomenon of the QHE breakdown

In this subsection, we report the finite excess noise at a V_{sd} smaller than V_{BD} . The excess noise shows a unique temporal variation on a time scale of minutes. We show our results of the noise measurement for the voltage-biased QHE state. Then, we discuss the possible origin of the excess noise by considering the precursor phenomenon of the QHE breakdown.

1. Finite excess noise in the precursor regime

Figure 7(a) shows $G(V_{sd})$ and $S(V_{sd})$ as a function of the normalized source-drain bias voltage (V_{sd}/V_{BD}) obtained around the $\nu = 2$ QHE state. Data obtained at $B = 4.2, 4.0,$ and 3.8 T are plotted as circles, triangles, and squares, respectively. Those plots have almost the same V_{sd} dependence, which is described as follows: At $V_{sd}/V_{BD} = 1$, $G(V_{sd})$ deviates from $2e^2/h$ and $S(V_{sd})$ increases abruptly, owing to the QHE breakdown. An important characteristic of $S(V_{sd})$ is the finite excess noise at $V_{sd} < V_{BD}$. Typically, the excess noise reaches about $0.6 \times 10^{-27} \text{ A}^2/\text{Hz}$ at $V_{sd}/V_{BD} = 0.95$. This is about an order smaller than the value reached in the breakdown regime.

The finite excess noise is also observed in the vicinity of the $\nu = 1$ QHE state. Figure 7(b) shows data obtained

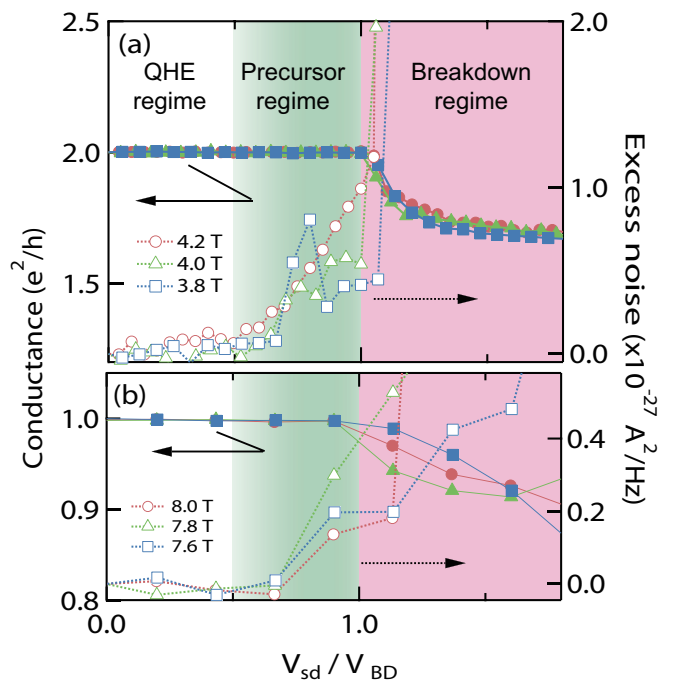


FIG. 7. (Color online) $G(V_{sd})$ and $S(V_{sd})$ as a function of V_{sd} obtained at (a) $\nu \sim 2$ and (b) $\nu \sim 1$. The range of V_{sd} is divided into a “QHE regime,” a “precursor regime,” and a “breakdown regime.”

at $B = 8.0, 7.8,$ and 7.6 T. In spite of the low density of data points, finite excess noise is always observed at V_{sd} smaller than V_{BD} . A typical value of $S(V_{sd})$ is about $0.2 \times 10^{-27} \text{ A}^2/\text{Hz}$ at $V_{sd}/V_{BD} = 0.90$.

To clarify the following discussion, we divide V_{sd} into three regions: the “QHE regime,” the “precursor regime,” and the “breakdown regime,” as shown in Fig. 7. In the QHE regime (typically, at $V_{sd}/V_{BD} \lesssim 0.5$), $G(V_{sd})$ is quantized and $S(V_{sd})$ is strongly suppressed. In the precursor regime, although $G(V_{sd})$ is still quantized, finite $S(V_{sd})$ is observed even when V_{sd} is smaller than V_{BD} . At $V_{sd}/V_{BD} > 1$, the QHE breakdown causes $G(V_{sd})$ to deviate from the quantized value.

The V_{sd} dependence of $S(V_{sd})$ is different in the three V_{sd} regions. In the QHE regime, even though $S(V_{sd})$ is strongly suppressed, a small, finite $S(V_{sd})$ of less than $10^{-28} \text{ A}^2/\text{Hz}$ is observed. $S(V_{sd})$ shows a clear quadratic V_{sd} dependence. Hence, we conclude that $S(V_{sd})$ in the QHE regime originates from Joule heating at the ohmic contacts. The quadratic V_{sd} dependence deviates in the precursor regime because of additional noise. The emergence of this additional noise is not transitional but appears as a “crossover.” Therefore, the boundary between the QHE regime and the precursor regime is not clear. In contrast, the boundary between the precursor state and the breakdown state is obvious, as the QHE breakdown is a transition. In the breakdown regime, $S(V_{sd})$ is almost constant.

Because the additional excess noise in the precursor

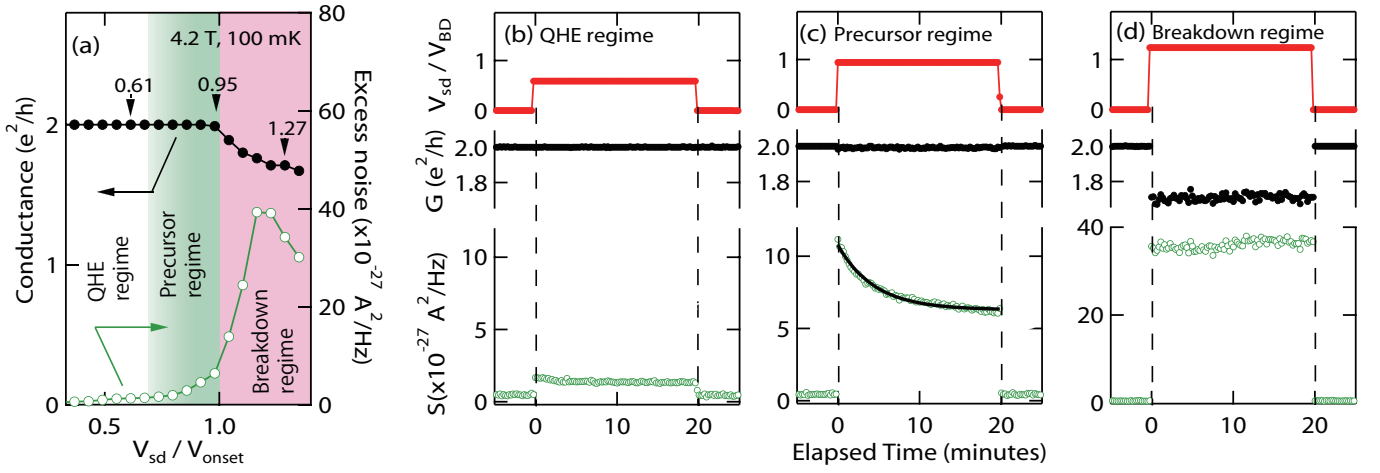


FIG. 8. (Color online) (a) $G(V_{sd})$ and $S(V_{sd})$ as a function of V_{sd}/V_{BD} ($V_{BD} = 16.5$ mV). (b)–(d) V_{sd} , $G(V_{sd})$, and $S(V_{sd})$ as a function of the elapsed time. V_{sd}/V_{BD} was set to (b) 0.61, (c) 0.95, and (d) 1.27 from 0.00 at the elapsed time $t = 0$ min. Then, V_{sd}/V_{BD} was set to 0 at $t = 20$ min. The solid line in (c) is a fitting curve with the exponential fitting function. All the measurements were performed at $B = 4.2$ T and $T = 100$ mK.

regime is universally observed in different Landau fillings (see Fig. 7), the excess noise is related to the universal behavior of the QHE regime. Next, we investigate $S(V_{sd})$ behavior in the precursor regime to clarify the origin of the additional excess noise.

2. Temporal variation of the excess noise

The excess noise in the precursor regime exhibits unique temporal variation. To investigate the excess noise dynamics in the precursor regime, the following three-step scheme was executed. First, V_{sd}/V_{BD} is set as 0.0 for a long time. Second, V_{sd}/V_{BD} is set to x ($x = 0.36, 0.42, 0.48,$ and 1.33) at the elapsed time $t = 0$ s. Finally, at $t = 20$ min, V_{sd}/V_{BD} is again set to 0.0.

Figure 8(a) shows $G(V_{sd})$ and $S(V_{sd})$ for different cooling downs as a function of V_{sd}/V_{BD} at $B = 4.2$ T and $T = 100$ mK. In this case, $V_{BD} = 16.5$ mV.

Figure 8(b)–(d) shows $V_{sd}(t)$, $G(V_{sd}, t)$, and $S(V_{sd}, t)$ as a function of time t obtained by the three-step scheme. Here, we focus on the dynamics of $S(V_{sd}, t)$. In the QHE regime [see Fig. 8(b)], $S(V_{sd}, t)$ is almost constant. In the precursor regime [see Fig. 8(c)], $S(V_{sd}, t)$ shows temporal variation on a time scale of minutes. In the breakdown regime [see Fig. 8(d)], $S(V_{sd}, t)$ does not exhibit temporal variation.

The temporal variation of $S(V_{sd}, t)$ in the precursor regime is analyzed with the exponential fitting function $S(t) = A \exp(t/\tau) + B$, where A is the amplitude of the time-dependent component of the excess noise, τ is the time scale of the temporal variation, and B is the background noise amplitude. From the analysis, the typical time scale of the temporal variation is obtained as $\tau \sim 200 \pm 100$ s.

Figure 9 shows A as a function of V_{sd}/V_{BD} . This is

analyzed by using an exponential fitting function with a fixed value of $\tau = 200$ s. A is zero in the QHE regime. It becomes finite at $V_{sd}/V_{BD} \sim 0.7$ and exhibits a maximum around $V_{sd}/V_{BD} = 0.9$. In the breakdown regime, A decreases rapidly.

This temporal variation of $S(V_{sd}, t)$ in the precursor regime indicates that some slow dynamics is involved in the electron transport. We discuss the origin of the temporal variation in the later text.

3. Relaxation behavior of the excess noise

Relaxation of the temporal variation of the excess noise is also observed with a pump-probe scheme. This scheme has three steps as follows: First, the excess noise is saturated in the precursor regime (at $V_{sd}/V_{BD} = 0.79$ for 600 s). Then, the system is relaxed at $V_{sd}/V_{BD} = 0.0$ for a wait time τ_w . Next, V_{sd}/V_{BD} is set to the initial value

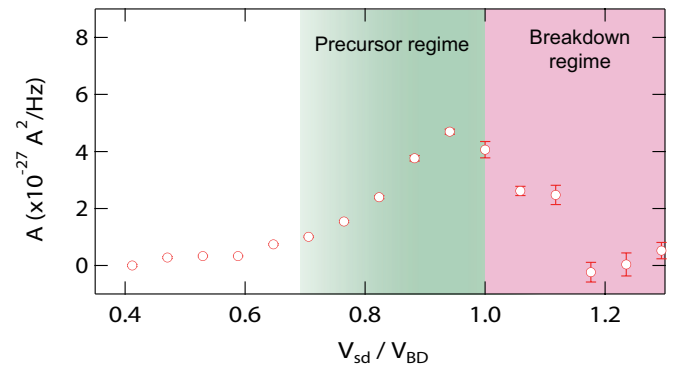


FIG. 9. (Color online) Amplitude of time-dependent component of the excess noise as a function of V_{sd}/V_{BD} .

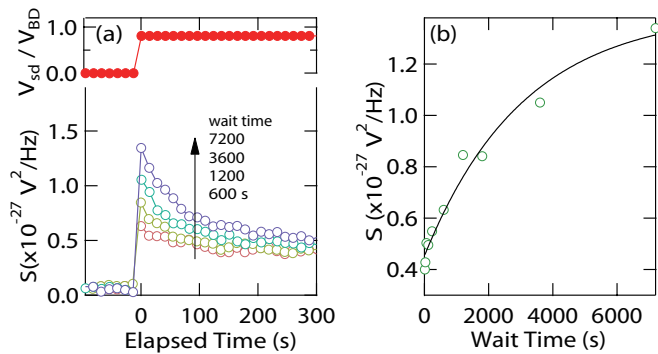


FIG. 10. (Color online) (a) $S(V_{sd})$ as a function of t . After S was saturated at $V_{sd}/V_{BD} = 0.79$, V_{sd}/V_{BD} was set as 0.00 for the wait time. Then, V_{sd}/V_{BD} was set to 0.79 at $t = 0$ s. (b) $S(V_{sd})$ at $t = 0$ s as a function of the wait time. The solid curve is the result of the fitting by a single exponential fitting function.

($V_{sd}/V_{BD} = 0.79$) at elapsed time $t = 0$ s. Figure 10(a) shows $V_{sd}(t)$ and $S(V_{sd}, t)$ as a function of t in the pump-probe scheme. After relaxation at $V_{sd}/V_{BD} = 0.00$ for τ_w , V_{sd} is changed from $V_{sd}/V_{BD} = 0.00$ to 0.79 at $t = 0$ s. The excess noise shows a τ_w dependence; the excess noise at $t = 0$ s increases as τ_w increases. This behavior of excess noise indicates that the temporal variation of the excess noise originates from the tunneling of transport electrons to some trapping sites with a long time constant.

Figure 10(b) shows the excess noise at $t = 0$ s as a function of τ_w . We analyzed it with the exponential fitting function $S(t) = A \exp(t/\tau_r) + B$, where τ_r is the time scale of the relaxation. τ_r is determined to be about 3000 s. It is longer than that of the temporal variation in Fig. 8(c). Such a difference between the time constants may imply the existence of a rate-limiting relaxation process.

C. Possible mechanism of the precursor phenomenon

Let us start by discussing characteristics of electron transport in the QHE regime. In this regime, electrons flow in the conductive edge channels. Counterflowing channels are spatially separated by the bulk insulating state, as Halperin demonstrated.³ Hence, backscattering of electrons is strongly suppressed. In the bulk, electrons and holes are localized in puddles with a typical size on the order of 100 nm.^{53,54} This conductive edge and insulating bulk picture is schematically shown in Fig. 11(a). The Fermi surface is placed at the zero-gap metallic state at the edge and at the energy gap in the bulk. This energy gap protects the electrons being transported by backscattering.⁴

The edge transport of the QHE state breaks down according to the following scenario.³³ First, electrons in the edge state tunnel to the localized bulk state. The excited electrons are accelerated by the Hall electric field.

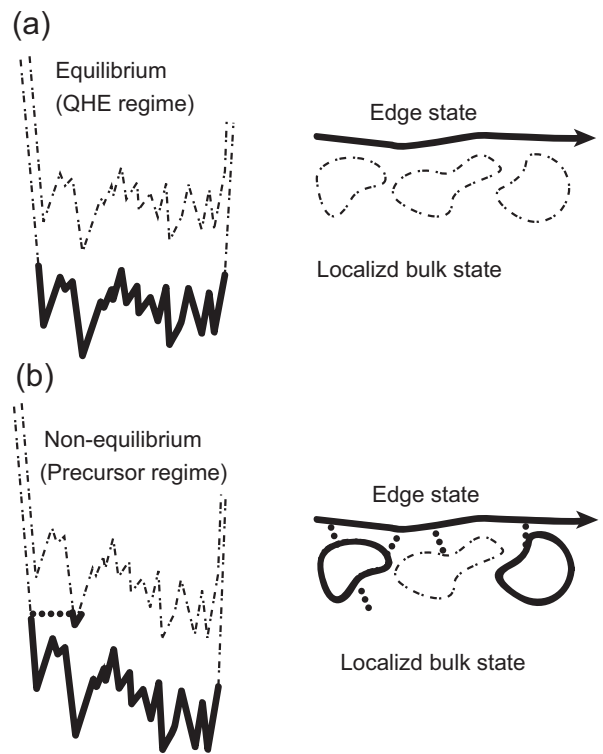


FIG. 11. Schematic illustration of the edge states and the localized bulk states in (a) the QHE regime and (b) the precursor regime. Left panel: energy-position plot; the vertical axis is the energy and the horizontal axis is the position across the counterflowing edge channels. Right panel: real space image of the edge and the bulk states. The dashed curve and the solid curve represent unoccupied states and occupied states, respectively. The dotted line denotes electron tunneling between the edge state and the bulk states.

When the accelerated electrons derive sufficient energy to generate new excited electrons, there is generation of conduction electrons during electron scattering. As a result of the multiplication of this process, a large number of conduction electrons are generated in the bulk. This avalanche-type generation of conduction electrons in the bulk is the QHE breakdown.

From this scenario of the QHE breakdown, the presence of electron tunneling without the avalanche is reasonable and we believe that this is what we observe in the precursor regime. A schematic image of the QHE state is shown in Fig. 11(b). In this V_{sd} region, electrons tunnel back and forth between the edge states and the localized puddles. When V_{sd} becomes larger than V_{BD} , the electrons in the bulk generate the avalanche and the QHE state breaks down.

The origin of the temporal variation of $S(V_{sd})$ lies in the transient behavior of the electron tunneling. When the tunneling starts, the localized bulk states are empty. As electrons tunnel back and forth between the edge states and the localized bulk states, the number of available unoccupied localized bulk states decreases. This de-

crease in the number of empty localized bulk state results in the reduction of the tunneling probability. Our observation of the temporal variation of $S(V_{sd})$ is explained as follows: First, $S(V_{sd})$ is large because the tunneling probability of the conduction electron is large. As the number of unoccupied localized bulk states decrease, the probability of electron tunneling and $S(V_{sd})$ decrease. Within a few minutes, the number of unoccupied localized bulk states in the bulk reaches steady state, resulting in a constant value of $S(V_{sd})$. This dynamics should be affected by the filling of the Landau level.

The origin of the excess noise in the precursor regime is not simply a result of the electron tunneling itself as the excess noise is frequency independent. The origin of the excess noise is likely to be caused by the increase in the effective electron temperature. The injection of hot electrons into the localized bulk state through electron tunneling increases the effective electron temperature inside the bulk state, and electron tunneling between the edge state and the bulk state results in the broadening of the energy distribution inside the edge state. The broadening of the energy distribution is observed as a finite increase in $S(V_{sd})$ in the voltage-biased QHE state.

Although other possible origins of the temporal variation of $S(V_{sd})$ could be Joule heating, dynamic nuclear polarization (DNP)^{45,55,56}, or the DX center,^{57,58} they are all inapplicable in this case. First, because the time dependence of the excess noise is only observed in the precursor regime, Joule heating is not a plausible explanation for the phenomenon. Second, $S(V_{sd})$ shows no response to microwave irradiation at the nuclear magnetic resonance (NMR) frequency.⁵⁹ If DNP is generated in the precursor regime, the excess noise should respond to the microwave irradiation at the NMR frequency. Hence, we conclude that the nuclear spin is not related to the excess noise generation. Third, the precursor regime is

universally observed immediately before the onset of the QHE breakdown. The scale of V_{sd} changes as we modify B . This indicates that the precursor phenomenon is not related to an impurity-induced phenomenon, which should have a specific energy scale.

IV. SUMMARY

We performed noise measurements for a device in a nonequilibrium quantum Hall effect (QHE) state and identified two distinct components of excess noise. The first one originates from avalanche-type electron heating of the QHE breakdown. The other is generated by electron tunneling without the avalanche of the conduction electrons in the bulk as a precursor of the QHE breakdown. This electron tunneling has long time constants, on the scale of minutes. The slow dynamics is observed as a temporal variation of the excess noise. Although the occurrence of electron tunneling without an avalanche in the voltage-biased QHE state seems plausible, such a slow dynamics has never been reported thus far. Because noise measurements offer us information on such elusive electron tunneling, the noise becomes a useful probe for studying the coupling between conductive states and their environment.

ACKNOWLEDGMENTS

We appreciate M. Hashisaka, Y. Yamauchi, S. Nakamura, Y. Tokura, K. Muraki, T. Fujisawa, K. Oto, and M. Kawamura for the fruitful discussions. This work is partially supported by the JSPS Funding Program for Next Generation World-Leading Researchers and a Grant-in-Aid for JSPS Fellows.

* chida@scl.kyoto-u.ac.jp

¹ K. von Klitzing, G. Dorda, and M. Pepper, *Phys. Rev. Lett.* **45**, 494 (1980).

² D. J. Thouless, M. Kohmoto, M. P. Nightingale, and M. den Nijs, *Phys. Rev. Lett.* **49**, 405 (1982).

³ B. I. Halperin, *Phys. Rev. B* **25**, 2185 (1982).

⁴ M. Büttiker, *Phys. Rev. B* **38**, 12724 (1988).

⁵ D. B. Chklovskii, K. A. Matveev, and B. I. Shklovskii, *Phys. Rev. B* **47**, 12 605 (1993).

⁶ J. Weis and K. von Klitzing, *Phil. Trans. R. Soc. A* **369**, 3954 (2012).

⁷ I. Neder, M. Heiblum, Y. Levinson, D. Mahalu, and V. Umansky, *Phys. Rev. Lett.* **96**, 016804 (2006).

⁸ Y. Yamauchi, M. Hashisaka, S. Nakamura, K. Chida, S. Kasai, T. Ono, R. Leturcq, K. Ensslin, D. C. Driscoll, A. C. Gossard, and K. Kobayashi, *Phys. Rev. B* **79**, 161306(R) (2009).

⁹ L. V. Litvin, H.-P. Tranitz, W. Wegscheider, and C. Strunk, *Phys. Rev. B* **75**, 033315 (2007).

¹⁰ P. Roulleau, F. Portier, D. C. Glatli, P. Roche, A. Cavanna, G. Faini, U. Gennser, and D. Mailly, *Phys. Rev. Lett.* **100**, 126802 (2008).

¹¹ L. V. Litvin, A. Helzel, H.-P. Tranitz, W. Wegscheider, and C. Strunk, *Phys. Rev. B* **78**, 075303 (2008).

¹² I. P. Levkivskiy and E. V. Sukhorukov, *Phys. Rev. B* **78**, 045322 (2008).

¹³ S. C. Youn, H.W. Lee, and H. S. Sim, *Phys. Rev. Lett.* **100**, 196807 (2008).

¹⁴ D. T. McClure, Y. Zhang, B. Rosenow, E. M. Levenson-Falk, C. M. Marcus, L. N. Pfeiffer, and K.W. West, *Phys. Rev. Lett.* **103**, 206806 (2009).

¹⁵ C. Altimiras, H. le Sueur, U. Gennser, A. Cavanna, D. Mailly, and F. Pierre, *Nat. Phys.* **6**, 34 (2010).

¹⁶ H. le Sueur, C. Altimiras, U. Gennser, A. Cavanna, D. Mailly, and F. Pierre, *Phys. Rev. Lett.* **105**, 056803 (2010).

¹⁷ C. Altimiras, H. le Sueur, U. Gennser, A. Cavanna, D. Mailly, and F. Pierre, *Phys. Rev. Lett.* **105**, 226804 (2010).

¹⁸ H. Kamata, T. Ota, K. Muraki, and T. Fujisawa, *Phys. Rev. B* **81**, 085329 (2010).

- ¹⁹ N. Kumada, H. Kamata, and T. Fujisawa, *Phys. Rev. B* **84**, 045314 (2011).
- ²⁰ G. Ebert, K. von Klitzing, K. Ploog, and G. Weimann, *J. Phys. C* **16**, 5441 (1983).
- ²¹ M. E. Cage, R. F. Dziuba, B. F. Field, E. R. Williams, S. M. Girvin, A. C. Gossard, D. C. Tsui, and R. J. Wagner, *Phys. Rev. Lett.* **51**, 1374 (1983).
- ²² M. Z. Hasan, and C. L. Kane, *Rev. Mod. Phys.* **82**, 3045 (2010).
- ²³ D. C. Tsui, G. J. Dolan, and A. C. Gossard, *Bull. Am. Phys. Soc.* **28**, 336 (1983).
- ²⁴ S. A. Trugman, *Phys. Rev. B* **27**, 7539 (1983).
- ²⁵ P. Streda and K. von Klitzing, *J. Phys. C* **17**, L483 (1984).
- ²⁶ O. Heinonen, P. L. Taylor, and S. M. Girvin, *Phys. Rev. B* **30**, 3016 (1984).
- ²⁷ L. Eaves and F.W. Sheard, *Semicond. Sci. Technol.* **1**, 346 (1986).
- ²⁸ M. I. Dyakonov, *Solid State Commun.* **78**, 817 (1991).
- ²⁹ C. Chaubet, A. Raymond, and D. Dur, *Phys. Rev. B* **52**, 11178 (1995).
- ³⁰ C. Chaubet and F. Geniet, *Phys. Rev. B* **58**, 13015 (1998).
- ³¹ V. Tsemekhman, K. Tsemekhman, C. Wexler, J.H. Han, and D.J. Thouless, *Phys. Rev. B* **55**, 10201(R) (1997).
- ³² S. Komiyama, T. Takamasu, S. Hiyamizu, and S. Sasa, *Solid State Commun.* **54**, 479 (1985).
- ³³ S. Komiyama and Y. Kawaguchi, *Phys. Rev. B* **61**, 2014 (2000).
- ³⁴ S. Komiyama, Y. Kawaguchi, T. Osada, and Y. Shiraki, *Phys. Rev. Lett.* **77**, 558 (1996).
- ³⁵ I. I. Kaya, G. Nachtwei, K. von Klitzing, and K. Eberl, *Phys. Rev. B* **58**, 7536(R) (1998).
- ³⁶ I. I. Kaya, G. Nachtwei, K. von Klitzing, and K. Eberl, *Europhys. Lett.* **46**, 62 (1999).
- ³⁷ B. E. Sağol, G. Nachtwei, K. von Klitzing, G. Hein, and K. Eberl, *Phys. Rev. B* **66**, (2002) 075305.
- ³⁸ Y. Kawaguchi, F. Hayashi, S. Komiyama, T. Osada, Y. Shiraki, and R. Itoh, *Jpn. J. Appl. Phys., Part 1* **34**, 4309 (1995).
- ³⁹ G. Nachtwei, *Physica E* **4**, 79 (1999), and references therein.
- ⁴⁰ Y. M. Blanter and M. Büttiker, *Phys. Rep.* **336**, 1 (2000).
- ⁴¹ M. Büttiker, *Phys. Rev. Lett.* **65**, 2901 (1990).
- ⁴² Note that the device shows the asymmetric QHE breakdown. It is understood as the difference of confinement potential steepness between the electrically defined edge and the etching-defined one [A. Siddiki, J. Horas, D. Kupidura, W. Wegscheider and S. Ludwig, *New J. Phys.* **12**, 113011 (2010)].
- ⁴³ M. Hashisaka, Y. Yamauchi, S. Nakamura, S. Kasai, K. Kobayashi, and T. Ono, *J. Phys.: Conf. Ser.* **109**, 012013 (2008).
- ⁴⁴ M. Hashisaka, Y. Yamauchi, K. Chida, S. Nakamura, K. Kobayashi, and T. Ono, *Rev. Sci. Instrum.* **80**, 096105 (2009).
- ⁴⁵ K. Chida, M. Hashisaka, Y. Yamauchi, S. Nakamura, T. Arakawa, T. Machida, K. Kobayashi, and T. Ono, *Phys. Rev. B* **85**, 041309(R) (2012).
- ⁴⁶ M. Hashisaka, S. Nakamura, Y. Yamauchi, S. Kasai, K. Kobayashi, and T. Ono, *Phys. Status Solidi C* **5**, 182 (2008).
- ⁴⁷ L. DiCarlo, Y. Zhang, D. T. McClure, C. M. Marcus, L. N. Pfeiffer, and K. W. West, *Rev. Sci. Instrum.* **77**, 073906 (2006).
- ⁴⁸ Y. Nishihara, S. Nakamura, K. Kobayashi, T. Ono, M. Kohda, and J. Nitta, *Appl. Phys. Lett.* **100**, (2012) 203111.
- ⁴⁹ This temperature results from the heat current through the signal line for the resistive-detection NMR. Without the signal line, the base electron temperature of the setup is below 20 mK.
- ⁵⁰ K. Sekiguchi, T. Arakawa, Y. Yamauchi, K. Chida, M. Yamada, H. Takahashi, D. Chiba, K. Kobayashi, and T. Ono, *Appl. Phys. Lett.* **96**, 252504 (2010).
- ⁵¹ T. Arakawa, K. Sekiguchi, S. Nakamura, K. Chida, Y. Nishihara, D. Chiba, K. Kobayashi, A. Fukushima, S. Yuasa, and T. Ono, *Appl. Phys. Lett.* **98**, 202103 (2011).
- ⁵² T. Tanaka, T. Arakawa, K. Chida, Y. Nishihara, D. Chiba, K. Kobayashi, T. Ono, H. Sukegawa, S. Kasai, and S. Mitani, *Appl. Phys. Express* **5**, 053003 (2012).
- ⁵³ G. Finkelstein, P. I. Glicofridis, R. C. Ashoori, and M. Shayegan, *Science* **289**, 90 (2000).
- ⁵⁴ N. B. Zhitenev, T. A. Fulton, A. Yacoby, H. F. Hess, L. N. Pfeiffer, and K. W. West, *Nature* **404**, 473 (2000).
- ⁵⁵ M. Kawamura, H. Takahashi, K. Sugihara, S. Masubuchi, K. Hamaya, and T. Machida, *Appl. Phys. Lett.* **90**, 022102 (2007).
- ⁵⁶ T. Nakajima, Y. Kobayashi, S. Komiyama, and M. Tsuboi, T. Machida, *Phys. Rev. B* **81**, 085322 (2010).
- ⁵⁷ J. Kirtley, T. Theis, P. Mooney, and S. Wright, *J. Appl. Phys.* **63**, 1541 (1988).
- ⁵⁸ J. Müller, Y. Li, S. von Molnar, Y. Ohno, and H. Ohno, *Phys. Rev. B* **74**, 125310 (2006).
- ⁵⁹ Before the experiments, we observed the resistive-detection NMR in the breakdown regime of the $\nu \sim 1$ QHE state. At that time, we observed responses of the differential conductance and also the excess noise due to irradiation of microwaves in the frequency of the NMR.